RSC Advances

This article can be cited before page numbers have been issued, to do this please use: S. Chen, Y. Wu, Y. Zhao and D. Fang, *RSC Adv.*, 2015, DOI: 10.1039/C5RA13814K.

View Article Online
DOI: 10.1039/C5RA13814K

Graphical abstract

Deep blue organic light-emitting devices enabled by bipolar phenanthro[9,10-d]imidazole derivatives

Shuo Chen,[a] Yukun Wu,[b] Yi Zhao,*[,b] Daining Fang*[,a]

[a] *State Key Laboratory for Turbulence and Complex System, College of Engineering, Peking University, Beijing 100871, P. R .China*

[b] *State Key Laboratory on Integrated Optoelectronics, College of Electronics Science and Engineering, Jilin University, 2699 Qianjin Street, Changchun 130012, P. R. China*

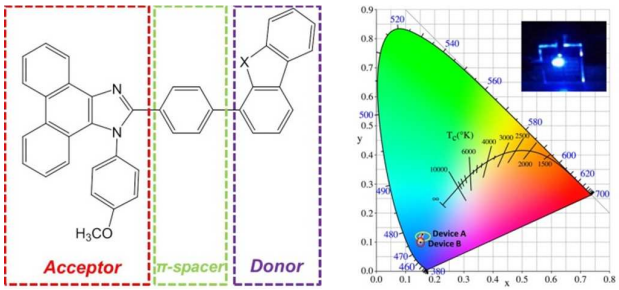

Novel phenanthroimidazole derivatives with D–π–A structure have successfully designed and prepared. Non-doped organic light emitting diodes (OLEDs) by employing the compounds display deep blue emission.

View Article Online
DOI: 10.1039/C5RA13814K

Deep blue organic light-emitting devices enabled by bipolar phenanthro[9,10-d]imidazole derivatives

Shuo Chen,[a, §] Yukun Wu,[b, §] Yi Zhao,*[,b] Daining Fang*[,a]

[a] *State Key Laboratory for Turbulence and Complex System, College of Engineering, Peking University, Chengfu Road, Beijing 100871, P. R .China*

[b] *State Key Laboratory on Integrated Optoelectronics, College of Electronics Science and Engineering, Jilin University, 2699 Qianjin Street, Changchun 130012, P. R. China*

[§] *These authors contributed equally.*

To whom the proofs and correspondence should be sent.

Associate Professor Daining Fang

College of Engineering

Peking University, Beijing, 100871, P. R. China

Fax: +86-010-62760322

E-mail: fangdn@pku.edu.cn

View Article Online
DOI: 10.1039/C5RA13814K

ABSTRACT

Two blue fluorescent phenanthroimidazole derivatives (**PhImFD** and **PhImTD**) with D–π–A structure by attaching the hole-transporting dibenzofuran or dibenzothiophene and electron-transporting phenanthroimidazole moieties are synthesized and characterized. Nonplanar twisted structures reduce molecular aggregations, which endows both of the compounds good thermal properties, film-forming abilities as well as high quantum yields in CH_2Cl_2 and in the solid state. Non-doped organic light emitting diodes (OLEDs) by employing the compounds **PhImFD** and **PhImTD** as emitters are fabricated and exhibited promising performance. The devices show the deep blue emission with the Commission Internationale de l'Eclairage (CIE) coordinates of (0.15, 0.11) for **PhImFD** and (0.15, 0.10) for **PhImTD**. **PhImFD** and **PhImTD** with the desired bipolar-dominant characteristics render the devices with a low driving voltage of 3.6 V. Energy levels of the materials were found to be related to the donor units in the compounds with different substituents. Device B using **PhImTD** as the emitting layer (EML) with fitly energy levels and increasing electron transport ability, possess favorable efficiencies of 1.34 cd m^{-2} for CE, 0.82 lm W^{-1} for PE and 1.63% for EQE. **PhImFD** and **PhImTD** are utilized as the blue emitter and the host for a yellow emitter PO-01 to fabricate white organic light-emitting diodes (WOLEDs), giving forward-viewing maximum CE of 8.12 cd m^{-2} and CIE coordinates of (0.339, 0.330). The results demonstrated not only phenanthroimidazole unit is an excellent block to construct deep blue emission materials, but also the chemical structure modification by introduction of suitable electron-donor substituent could influence the performance of device.

View Article Online
DOI: 10.1039/C5RA13814K

1. Introduction

Over recent decades, organic light-emitting diodes (OLEDs) have received increasing attention and expected to be used as next-generation lighting.[1] Owing to the advantages of planar lighting source, flexibility over a large area, mercury-free, low-cost fabrication, and high power-conversion efficiency, some tendency toward replacing the traditional light sources will gradually emerge.[2] On the commercial road, high efficiency and excellent stability are two constant goals. To achieve full-color electroluminescent displays, three color components, i.e., red, green, and blue, must be available.[3] As red and green light-emitting materials have acquired sufficient developments for commercial applying criteria of OLEDs,[4] the design and optimization of blue OLEDs has been remained a formidable challenge till date.[5] The blue emitter can not only effectively reduce power consumption of the devices but also be utilized to generate light of other colors by energy cascade to lower energy fluorescent or phosphorescent dopants.[6] Since Forrest *et al.* proposed the concept of phosphorescent OLEDs (PHOLEDs),[7] the introduction of phosphors can boost the internal quantum efficiency up to theoretical 100% through the use of triplet excitons for light emission.[8] However, it is much more difficult to find a blue phosphorescent emission with long lifetime and pure color Commission International de l'Eclairage (CIE), due to the inherent wide bandgap.[9] High CIE coordinates (y-coordinate > 0.25), short device lifetimes and environmental contaminants (heavy metals) are not suitable for them to be commercially used.[10] Therefore, in order to achieve marketable OLEDs, the hunt for highly efficient blue-fluorescent materials and devices still remains one of the most subject of current interest.

As known to all, the electron injection and transport ability in organic semiconductors is low compared to that of hole, the basic design for blue materials is to increase their electron affinities to realize balanced charge injection and transport. Therefore, the *n*-type imidazole moiety has been widely employed as an electron-transporting material and as the electron-withdrawing group of bipolar host material.[11] Meanwhile, phenanthroimidazole (PI) could readily construct a variety of

View Article Online
DOI: 10.1039/C5RA13814K

sky-blue and deep blue electroluminescent materials as the near-ultraviolet fluorescent chromophore.[12] While, PI including imidazole moiety can act as an electron-acceptor when linked with an electron-donating group, which exhibit an ambipolar characteristic.[13] Based on the inherent character of the imidazole group, deprotonation for the NH group on imidazole could be attached a wide variety of substituents, which be capable to inhibit strong π–π stacking and molecular interactions in the solid state.[14] Formation of smooth and stable amorphous films could be realized by the twisted configuration.[15] Simultaneously, the introduction of electron-deficient PI units effectively increases the electron injection and transport ability and facilely adjusts the ionization potentials (IP) of the compounds,[16] and further reduces the injection barrier at the interface between the hole transporting layer (HTL) and the emissive layer (EML) and balanced carriers recombination.[17] Actually, energy and charge transfer processes in the EML should be more accurately controlled to achieve low driving voltages and high efficiencies.[18] Therefore, developing high-efficiency deep blue OLEDs with a low driving voltage is of importance to promote the commercial applications in portable devices.[19]

Motivated by this research trend and our project on the synthesis of blue emitting compounds, the non-doped blue-fluorescent devices using phenanthroimidazole derivatives are reported. In this paper, we describe the design and synthesis of two bipolar phenanthroimidazole derivatives by using *para*-position of a freely rotatable phenyl bridge between the C-2 position of the imidazole ring and C-4 position of the dibenzofuran or dibenzothiophene. PI acts as a π–acceptor and can be incorporated to an electron donor to form bipolar molecule. We anticipate the rigid PI skeleton, as well as the freely rotatable aryl substituents on the C-2 positions of imidazole, are beneficial to the thermal and morphological stabilities without sacrificing the good electron-transport ability and high triplet energy imparted by PI unit. In addition, the bulk and sterically hindered molecular configuration is advantageous to effectively enhance photoluminescence quantum yield.[20] Thermal, photophysical, and electroluminescent properties of the compounds are comprehensively investigated. The new PI derivatives **PhImFD** and **PhImTD** possess high luminescent efficiency,

View Article Online
DOI: 10.1039/C5RA13814K

excellent luminous/thermo- stability and balanced injection and transport of charge carrier, which has opened us new opportunities in the utilization of PI derivatives for applications and functions.

2. Results and discussion

2.1 Synthesis

The synthetic route for **PhImFD** and **PhImTD** is shown in Scheme 1. The detailed procedures for the syntheses of the reaction intermediates and final products are depicted in synthesis part. **PhImFD** and **PhImTD** are composed of two main components: phenathroimidazole as the acceptor moiety and dibenzofuran and dibenzothiophene as the donor moiety. Firstly, **FD4B** and **TD4B** were achieved by bromination and borate acidification of dibenzofuran and dibenzothiophene at C-4 positions, respectively. The important precursor **PhImBr** was synthesized by one-pot cyclizing reaction in good yields.[21] This synthesis method could conveniently construct PI derivatives with various structures by tuning aromatic aldehyde and primary amine. The target molecules are obtained through the typical Suzuki cross-coupling reactions of the bromide intermediate **PhImBr** and the precursors **FD4B**/**TD4B** catalyzed by $Pd(PPh_3)_4$–NaOH in 79–82% yields. In order to pursue the maximized yields, the selective aprotic solvents THF, toluene and 1,4-dioxane were utilized for this reaction. The results prove that the utilization of THF can be able to contribute the maximized yields. The identities of **PhImFD** and **PhImTD** are established by ^{1}H NMR, ^{13}C NMR, high-resolution MS, and satisfactory elemental analysis data. Both of the molecules have well solubility in common organic solvents such as THF, dichloromethane, chloroform and toluene.

2.2 Thermal properties

The compounds **PhImFD** and **PhImTD** with dibenzofuran and dibenzothiophene at *para*-positions of the C2-phenyl and N1-phenyl of the phenanthroimidazole show high thermal stabilities. As illustrated in Fig. 1, the temperature of

View Article Online
DOI: 10.1039/C5RA13814K

thermal-decomposition (T_d, at weight loss of 5%) of **PhImFD** is 300°C, and **PhImTD** possesses a higher T_d of 318°C than **PhImFD**. The DSC results show that glass-transition temperature (T_g) of **PhImFD** and **PhImTD** are 110°C and 115°C, respectively, verifying that the small energetic disorder at the C2-phenyl of the phenanthroimidazole can efficiently enhance the morphological stability. The high T_d and T_g imply that they could form morphologically stable amorphous films upon thermal evaporation, which is a crucial parameter for applications of OLEDs.

2.3 Photophysical properties

The Ultraviolet-visible (UV–vis) absorption and photoluminescence (PL) emission spectra of **PhImFD** and **PhImTD** in dilute solution (10^{-5} mol L^{-1} in CH_2Cl_2) and film state were investigated photophysical properties (Fig. 2). The absorption spectra exhibit no distinct differences and both of the molecules exhibit four bands at *ca*. 265 nm, 290 nm, 333 nm and 365 nm in CH_2Cl_2 solution. The strong absorption bands at around 265 nm can be attributed to phenanthrene unit.[22] The absorption peaks at around 290 nm could be assigned to the dibenzofuran and dibenzothiophene centered n–π* transition.[23] The absorption bands at 333 nm might be due to the π–π* transition of the substituent on the 2-imidazole position to the PI unit.[24] The weak peaks at 365 nm were originated from the π–π* transition of PI unit. Moreover, the optical bandgap in solution were 3.19 and 3.17 eV for **PhImFD** and **PhImTD**, estimated by the absorption edge. The photophysical data for emission are gathered in Table 1. Corresponding emission peaks of **PhImFD** and **PhImTD** in CH_2Cl_2 appeared at 421 and 423 nm, respectively. As expected, the emission maxima of **PhImFD** and **PhImTD** in a thin film (both at 440 nm) are bathochromic shifted by *ca*. 18 nm compared with those peaks in solution, which is likely to be caused by π–π stacking and intermolecular aggregation of bulky existing in the form of solid.[25] **PhImFD** and **PhImTD** show high PL quantum yields of 0.58 and 0.62 in the CH_2Cl_2 solution, respectively. While the corresponding quantum yields for powder are 0.39 and 0.44 for **PhImFD** and **PhImTD**, showing the potential application in OLEDs. In

View Article Online
DOI: 10.1039/C5RA13814K

addition, in order to investigate the triplet energy level, cryogenic temperature (77 K) time-resolved phosphorescent spectra measurements were also performed in 2-methyl-THF glasses (Fig. S16), which were determined as 2.99 and 3.03 eV according to 0–0 transitions.

2.4 Theoretical calculation

Density Functional Theory (DFT) calculations (B3LYP/6-31G(d)) were carried out to investigate the structure-property relationship of the new compounds. Fig. 3 shows the highest occupied molecular orbital (HOMO) and the lowest unoccupied molecular orbital (LUMO) distribution of **PhImFD** and **PhImTD**. The electron clouds of HOMO of **PhImFD(TD)** was distributed on the **FD(TD)** unit because of the electron-rich dibenzofuran and dibenzothiophene unit, and the electron clouds of LUMO of **PhImFD(TD)** was dispersed over the PI and extended phenyl unit owing to the electron-deficient imidazole unit. The HOMO and LUMO of **PhImFD** and **PhImTD** were completely separated, indicating that HOMO–LUMO excitation would shift the electron density distribution from one side of the dibenzofuran and dibenzothiophene groups as the donor to the other side phenanthroimidazole as the acceptor. This observations are in accord with the fact that BF(TD) is a hole transport unit and PI is an electron transport unit for **PhImFD(TD)**. Moreover, the dihedral angels between the adjacent phenyl linker and phenanthroimidazole are 29.5° and 29.1° for **PhImFD** and **PhImTD**, respectively. Closer inspection reveals the conjugated phenyl linker and the adjacent BF and TD planes intersect with the approximately perpendicular dihedral angels (84.5° and 87.1° for **PhImFD** and **PhImTD**, respectively).

2.5 Electrochemical properties

Fig. 4 reveals the bipolar electrochemical character of **PhImFD** and **PhImTD**, as evidenced using cyclic voltammetry (CV) measurements. The electrochemical data are summarized in Table 1. The HOMO energy levels of the compounds were

View Article Online
DOI: 10.1039/C5RA13814K

determined from the onset of first oxidation potentials with regard to the energy level of SCE (assuming that the absolute energy level of the Fc/Fc^+ redox couple was 4.4 eV below cacuum). We observed one reversible oxidation potential at 0.6 V for **PhImFD** and 1.09 V for **PhImTD**. Through subtraction of the optical energy gap (E_g) from the HOMO energy level, we calculated the energy level of the LUMO to be –1.81 and –2.32 eV for **PhImFD** and **PhImTD**, respectively. The molecular orbital data indicate that the HOMO/LUMO level of dibenzothiophene substituted derivatives are obviously lower than those of the dibenzofuran substituted one. The differences of energy level depend on the linkage units of the electronic donor moieties, because the dibenzofuran is a weaker electron donor than dibenzothiophene group and molecules end-capped with dibenzothiophene are more coplanar according to the DFT calculations. More importantly, no electropolymerization occurred during multiple cycles of CV scanning. Thus, the appending of the electron-accepting phenanthroimidazole units onto the dibenzofuran and dibenzothiophene renders **PhImFD** and **PhImTD** with promising electrochemical stability and bipolar characteristics, which may interpret a greater separation of the HOMO and LUMO orbitals,[26] which is in good agreement with the result of the DFT calculations.

2.6 Electroluminescent properties

To evaluate the performance of **PhImFD** and **PhImTD** as emitters, multilayer OLED devices A and B were fabricated (see Fig. 5 for device configurations). Devices A and B had compounds **PhImFD** and **PhImTD**, respectively, as emitters. The EL spectra, luminance and current density *vs*. applied voltage, and current efficiency (CE), power efficiency (PE) and external quantum efficiency (EQE) vs. luminance of devices A and B are displayed in Figs. 6–8. The key performance parameters of the devices are summarized in Table 2. Devices A and B with the structure ITO/MoOx (2nm)/NPB (40nm)/PhImFD or PhImTD (30nm)/TPBi (40nm)/LiF (1nm)/Al (100nm) (ITO is indium tin oxide, NPB is *N,N′*-Bis-(1-naphthalenyl)-*N,N′*-bis-phenyl-(1,1'-biphenyl)-4,4'-diamine, and TPBi is

View Article Online
DOI: 10.1039/C5RA13814K

1,3,5-Tri(1-phenyl-1H-benzo[*d*]imidazol-2-yl)phenyl) are produced. MoOx is utilized as a hole-injecting layer, and NPB and TPBi are selected as a hole and electron-transporting layers, respectively. Both of the devices exhibit deep blue EL spectra with the peak wavelength at 445 nm, which shows no little vibronic feature (Fig. 6). The EL spectra of the devices are almost the same as their corresponding photoluminescent spectra in the film state, indicating the EL spectra are indeed from the emitting layers with no excimer or exciplex emission. Importantly, the saturated deep blue EL emissions are quite stable under the applied voltages ranged from 6 to 10 V. Full width at half maximum (FWHM) is around 70 nm and the CIE y coordinate value < 0.12 along with an (x+y) value < 0.28 are achieved which effectively guarantees the saturated deep blue colors, which remains almost unchanged over a range of luminance from 1000 cd^{-2} m to 3000 cd m^{-2}. In addition, device B exhibits evidently better performance as compared with device A. It is well known that efficient carrier injection at interfaces between different layers in OLEDs is essential for obtaining high performance devices. Thus, it is crucial for the EML to possess a shallow HOMO for facilitating hole-injection. However, compared with that of **PhImFD**, HOMO/LUMO of **PhImTD** is even more remarkably reduced, by 0.5 eV. On the one hand, the hole injection barriers between **PhImTD** and the HTL are very small (0.1 eV). On the other hand, the LUMO energy of **PhImTD** (–2.3 eV) are close to that of TPBi (–2.7 eV), and the electron injection barriers between **PhImFD** and the TPBi are much too big (0.9 eV), which reveals that the electron injection ability of **PhImTD** is relatively easier than that of **PhImFD**. That is reasonable as the dibenzothiophene substituted phenanthroimidazole have a lower HOMO/LUMO fit HTL and ETL better when compared with the dibenzofuran substituted one. The results reflect the dibenzothiophene as the donor unit affords more appropriate HOMO/LUMO level, which features the preference of balanced carrier injection and transporting. Meanwhile, it gives us a new method to introduce building block to tune the HOMO/LUMO energies. To further understand both hole and electron injection/transport characteristics of **PhImFD** and **PhImTD**, the single-carrier devices are fabricated (Fig. S10). The current density-voltage (J–V) characteristics illustrate

View Article Online
DOI: 10.1039/C5RA13814K

that hole current density values of **PhImFD** and **PhImTD** are not much different but the electron current density values of **PhImTD** are higher than that of **PhImFD**, which is probably caused by the excellent electron transporting for **PhImTD**. **PhImTD** has bipolar charge transporting capacity as evidenced by the considerable hole/electron current density, which results that the charge transporting property **PhImTD** is superior to that of the **PhImFD**. As depicted in Fig. 8, device B gives the performance in terms of a maximum EQE of 1.63 %, a maximum CE of 1.34 cd A^{-1} and a maximum PE of 0.82 lm W^{-1}. Although performance of the deep blue devices is lower than that of PI-based device, it is improved in comparison with those of PI-based devices substituted carbazole.[24] The CIE coordinates is located at (0.151, 0.098) which mated well with the requirement of CIE deep blue criterion *y* coordinate value < 0.15 along with an (x+y) value < 0.30 (Fig. S11).

The field of white organic light emitting devices (WOLEDs) has inspired research activities on the bases of their great potential in the lighting system. The WOLEDs is generally realized by mixing red, green and blue emitters in a certain ratio, or by two complementary colors (orange or yellow and blue) providing the connection line of coordinates across the white light region. To fabricate doped WOLEDs, **PhImFD** and **PhImTD** were utilized as blue emitters, and PO-01 (acetylacetonatobis(4-phenylthieno[3,2-*c*]pyridinato-*N*,C2') Iridium) with an emission peak at 560 nm was utilized as the complementary yellow emitters. The typical EL spectra of the WOLEDs at different voltages are shown in Figs. S13 and S14. All the EL spectra could be divided into their blue emission corresponding to the fluorophore **PhImFD** and **PhImTD** and yellow emission corresponding to the phosphor PO-01. As a result, the device D employed **PhImTD** gave the best performance with the maximum luminance of 3095 cd m^{-2} and a maximum current efficiency of 8.12 cd A^{-1}, achieved, as shown in Fig. 9 and S12 and Table S2. Devices C and D exhibit a low turn-on voltage (< 3.7 V). The white light CIE coordinates of (0.339, 0.330) of device D at the luminance of 1000 cd m^2, which is very close to the standard white light point of (0.33, 0.33). In addition, a small offset of CIE coordinates of emitted light are observed under the various biases (at the luminance of 2000–6500 cd A^{-1}), which

View Article Online
DOI: 10.1039/C5RA13814K

reflects good color stability for doped WOLEDs. The inset of Fig. S15 is a snapshot of the WOLED at 14.0 V; a suitable white light emission with a uniform emitting area is seen.

3 Experimental sections

3.1 Materials and Instruments

All the reagents and solvents used for the synthesis of the compounds were purchased from Aldrich, Acros, J&K and TCI companies and used without further purification. Dopant material PO-01 was purchased from Lumtec Corp. (taiwan). ^{1}H and ^{13}C-nuclear magnetic resonance (NMR) spectra were recorded using a Bruker AVANCE III 500-MHz spectrometer at 500 MHz and 125MHz respectively, using DMSO-d_6 or $CDCl_3$ as the solvents and tetramethylsilane (TMS) as the internal standard. High resolution mass spectra were recorded on a Bruker APEX IV fourier transform ion cyclotron resonance mass spectrometer. Elemental analysis for C, H, and N were performed on a Perkin-Elmer 2400 automatic analyzer. All manipulations involving air-sensitive reagents were performed in an atmosphere of dry Ar. Absorption and photoluminescence (PL) emission spectra of the target compound were measured using a Perkin Elmer Lambda-750 UV-Vis-NIR spectrophotometer and LS 55 fluorescence spectrometer, respectively. Phosphorescence spectra were measured in CH_2Cl_2 using an Edinburgh FLS 920 fluorescence spectrophotometer at 77 K cooling by liquid nitrogen with a delay of 300 μs using Time-Correlated Single Photon Counting (TCSPC) method with a microsecond pulsed Xenon light source for 10 μs–10 s lifetime measurement. The luminescence quantum yields of compounds were measured at room temperature and cited relative to a reference solution of 9,10-dipenylanthracene (Φ = 0.9 in cyclohexane) as a standard, and they were calculated according to the well-known equation: $$\frac{\varphi_{overall}}{\varphi_{ref}} = \left(\frac{n}{n_{ref}}\right)^2 \frac{A_{ref}}{A} \frac{I}{I_{ref}} \quad (1)$$

In equation (1), n, A, and I denote the refractive index of solvent, the area of the emission spectrum, and the absorbance at the excitation wavelength, respectively, and

View Article Online
DOI: 10.1039/C5RA13814K

φ_{ref} represents the quantum yield of the standard 9,10-dipenylanthracene solution. The subscript *ref* denotes the reference, and the absence of a subscript implies an unknown sample. For the determination of the quantum yield, the excitation wavelength was chosen so that A < 0.05. For the solid samples, the quantum yields for the compounds were determined at room temperature through an absolute method using an Edinburgh Instruments' integrating sphere coupled to a modular Edinburgh FLS 920 fluorescence spectrophotometer. The values reported are the average of three independent determinations for each sample. The absolute quantum yield was calculated using the following expression (2): $\Phi = \frac{\int L_{emission}}{\int E_{reference} - \int E_{sample}}$. In expression (2), L_{emission} is the emission spectrum of the sample, collected using the sphere, E_{sample} is the spectrum of the incident light used to excite the sample, collected using the sphere, and $E_{\text{reference}}$ is the spectrum of the light used for excitation with only the reference in the sphere. The method is accurate to within 10%. Thermogravimetric analysis (TGA) and differential scanning calorimetry (DSC) were performed on Perkin Elmer TGA 4000 and DSC 8000 thermal analyzers under nitrogen atmosphere at a heating rate of 10 °C min^{-1}. Cyclic voltammetric (CV) measurements were carried out in a conventional three electrode cell using a Pt button working electrode of 2 mm in diameter, a platinum wire counter electrode, and a saturated calomel electrode (SCE) reference electrode on a computer-controlled CHI660d electrochemical workstation at room temperature. Reduction CV of all compounds was performed in CH_2Cl_2 containing teterabutylammonium hexafluorophosphate (Bu_4NPF_6, 0.1 M) as the supporting electrolyte. Ferrocene was used as an external standard. Electrochemistry was done at a scan rate of 100 mV/s.

3.2 Computational details

The theoretical investigation of geometrical properties was performed with the Gaussian 09 package.[27] Density functional theory (DFT) was calculated at Beck's three-parameter hybrid exchange functional[28] and Lee, and Yang and Parr correlation functional[29] B3LYP/6-31G (d). The spin density distributions were visualized using

View Article Online
DOI: 10.1039/C5RA13814K

Gaussview 5.0.8.

3.3 Device fabrication and measurement

Prior to the device fabrication, the patterned ITO-coated glass substrates were degreased with standard solvents, blow-dried using a N_2 gun, and exposed in a UV–ozone ambient for 30 min. All the organic layers were commercially purchased from Luminescence Technology Corp, and thermally deposited onto the ITO with a base pressure (~4.0×10^{-4} Pa) at a rate of 0.1–0.2 nm s^{-1} monitored in situ with the quartz oscillator. LiF covered by Al is used as cathode without breaking the vacuum. All the samples were measured directly after fabrication without encapsulation at room temperature under ambient atmosphere. The current-voltage-luminance characteristics were carried out using a PR655 Spectrascan spectrometer and a Keithley 2400 programmable voltage-current source. The external quantum efficiency (EQE) and luminous efficiency (LE) are calculated assuming Lambertian distribution, and then calibrated to the efficiencies obtained at 1000 cd m^{-2} in the integrating sphere (Jm-3200). The configurations of Device A and B were ITO/MoOx (2nm)/NPB (40nm)/PhImFD or PhImTD (30nm)/TPBi (40nm)/LiF (1nm)/Al (100nm), where MoOx and LiF anode/cathode buffer layer for hole/electron injection. NPB and TPBi served as hole- and electron-transporting layers (HTL and ETL), respectively. The nominal hole-only and electron-only devices were fabricated with the configurations of ITO/MoOx(2 nm)/NPB(40 nm)/PhImFD or PhImTD (30 nm)/NPB(40 nm)/MoOx(2 nm)/Al(100 nm) (hole-only transporting Device) and Al (100nm)/LiF (1nm)/TPBi(40 nm)/PhImFD or PhImTD (30 nm)/TPBi (40 nm)/ LiF (1nm)/Al (100nm) (electron-only transporting Device). The doped white OLEDs devices C and D are fabricated with the structure ITO/MoOx (2 nm)/NPB(40 nm)/PhImFD or PhImTD (15 nm)/PO-01(0.2nm)/PhImFD or PhImTD(15 nm)/TPBi (40 nm)/LiF (1 nm)/Al.

3.4 Synthesis

View Article Online
DOI: 10.1039/C5RA13814K

Synthesis of dibenzofuran-4-dioxaborolane (FD4B).

Dibenzofuran (11.76 g, 70 mmol) was dissolved in 100 mL of anhydrous THF and slowly lithiated with 1.6 M *n*-BuLi in hexane (44 mL, 70 mol) at −78 °C under an argon atmosphere. The solution was warmed to 0 °C and was stirred for 6 h. Afterward the reaction mixture was cooled to −78 °C and a solution of 1,2-dibromoethane (26.3 g, 140 mmol) in 20 mL anhydrous THF was added dropwise. The mixture was then stirred at room temperature for 10 h. After concentration under reduced pressure the crude brominated product was dissolved in CH_2Cl_2 and washed with water several times. The solution was concentrated again, and the resulting solid was recrystallized from an *n*-hexane/CH_2Cl_2 solution to give the 4-bromodibenzothiophene. Then, 4-bromodibenzothiophene (2.46 g, 10 mmol) was dissolved in 30 mL THF, and stirred with dry ice/acetone bath for 30 min. 9.4 mL *n*-BuLi (15mmol, 1.6M) in 30 mL THF was added dropwise to this solution. The solution was stirred for 2 h, and then trimethyl borate (3.4 mL, 30 mmol) was added to the solution, the solution was stirred for 1 h at −78 °C and warmed to r.t., and then cooled in an ice bath, and 2M HCl (30 mL, 60 mmol) added. and was stirred at r.t. for 8 hours. The mixture was diluted with CH_2Cl_2 and extracted three times with water. After being dried by anhydrous Na_2SO_4, the organic phase was completely removed by rotary evaporator to afford white dibenzofuran-4-boronic acid. A mixture of Pinacol (0.8863 g, 7.5 mmol) and dibenzofuran-4-boronic acid (1.0603 g, 5 mmol) in toluene (50 ml) was stirred at 80 °C overnight. Solvent was evaporated under reduced pressure and extracted with CH_2Cl_2/H_2O. The residue was purified by column chromatography using ethyl acetate/hexane (1:10) mixture as an eluent to give white powder. Yield: 86%. ^{1}H NMR (TMS, $CDCl_3$, 500 MHz): ppm δ = 8.05(d, J = 7.5 Hz, 1H); 7.91 (dd, *J* = 8.0 Hz, 2H); 7.66 (d, *J* = 8.0 Hz, 2H); 7.43 (t, *J* = 8.5 Hz, 1H); 7.36−7.30(m, 2H); 1.44 (s, 12H); HR-ESI-MS: $[M+H]^+$ m/z calcd for $C_{18}H_{20}BO_3$: 295.15074, found: 295.15032.

Synthesis of dibenzothiophene-4-dioxaborolane (TD4B).

The procedure for **TD4B** was similar as the preparation of **FD4B** starting from (12.86 g, 70 mmol) instead of dibenzofuran. Yield: 80%. ^{1}H NMR (TMS, $CDCl_3$, 500

View Article Online
DOI: 10.1039/C5RA13814K

MHz): ppm δ = 8.22(d, *J* = 8.0 Hz, 1 H); 8.11 (t, *J* = 6.5 Hz, 2 H); 8.90 (d, *J* = 7.5 Hz, 1 H); 7.84 (t, *J* = 4.0 Hz, 1 H); 7.45−7.40(m, 3 H); 1.35 (s, 12 H); HR-ESI-MS: $[M+H]^+$ m/z calcd for $C_{18}H_{20}BO_2S$: 311.12797, found: 311.12748.

Synthesis of 2-(4-Bromophenyl)-1-(4-methoxyphenyl)-1*H*-phenanthro[9,10-d]imidazole (PhImBr)

A mixture of 4-bromobenzaldehyde (248.3 mg, 13.5 mmol), phenanthrene-9,10-dione (280.9 mg, 13.5 mmol), 4-methoxy-benzenamin (830.7 mg, 67.5 mmol), ammonium acetate (354.2 mg, 54.5 mmol), and acetic acid (60 mL) were refluxed under nitrogen in an oil bath. After 24 h, the mixture was cooled and filtered. The solid product was washed with an acetic acid/water mixture (1:1, 100 mL) and water. It was then purified by chromatography using CH_2Cl_2/petroleum ether (1:1) as an eluent to obtain the product as green powder. Yield: 70%. ^{1}H NMR (TMS, $CDCl_3$, 500 MHz): ppm δ = 3.96 (s, 3H), 7.10 (d, *J*=8.5 Hz, 2H), 7.29 (t, *J*=7.0 Hz,2H), 7.39–7.45(m, 4H), 7.48–7.53 (m, 3H), 7.65(t, *J*=8.5 Hz, 1H), 7.73(t, *J*=7.0 Hz, 1H), 8.70 (d, *J*=8.0 Hz,1H), 8.76 (d, *J*=8.5 Hz, 1H), 8.84 (d, *J*=9.0 Hz, 1H); HR-ESI-MS: $[M+H]^+$ m/z calcd for $C_{28}H_{20}BrN_2O$: 479.07535, found: 479.07449.

Synthesis of 2-(4-bibenzofuran-4-phenyl)-1-(4-methoxyphenyl)-1H-phenanthro[9,10-d]imidazole (PhImFD)

A mixture of **PhImBr** (478.1 mg, 1 mmol), **FD4B** (294.1 mg, 1 mmol), tetrakis(triphenylphosphine)palladium (115.6 mg, 0.1 mmol), tetrabutylammonium bromide (32.2 g, 0.1 mmol), and aqueous solution of sodium hydroxide (2 mol L^{-1}, 6 mmol) in THF (20 mL) was stirred under argon at 80 °C for 48 h. After quenched with aqueous NH_4Cl solution, the mixture was extracted with CH_2Cl_2. The combined organic extracts were washed with brine and dried over anhydrous $MgSO_4$. After removing the solvent, the residue was purified by column chromatography on silica gel using CH_2Cl_2 as the eluent to give a white power. Yield: 82%. ^{1}H NMR (TMS, $CDCl_3$, 500 MHz): ppm δ = 3.96 (s, 3H), 7.14 (d, *J*=8.5 Hz, 2H), 7.28–7.43 (m, 4H), 7.46–7.54(m, 4H), 7.61(d, *J*=9.0 Hz, 2H), 7.66(t, *J*=7.5 Hz, 1H), 7.76 (t, *J*=7.0

View Article Online
DOI: 10.1039/C5RA13814K

Hz,1H), 7.81 (d, *J*=8.0 Hz,2H), 7.92 (dd, *J*=7.0 Hz, 3H), 7.98 (d, *J*=8.0 Hz, 1H), 8.71 (d, *J*=8.5 Hz, 1H), 8.78 (d, *J*=8.5 Hz, 1H), 8.93 (d, *J*=8.0 Hz, 1H); ^{13}C NMR (TMS, $CDCl_3$, 125 MHz): ppm δ = 160.43, 156.17, 153.30, 150.71, 136.73, 131.29, 130.10, 129.47, 128.57, 128.32, 127.30, 126.64, 126.32, 125.59, 125.07, 124.80, 124.12, 123.23, 123.11, 122.76, 120.86, 120.69, 119.98, 115.38, 111.86, 55.39; HR-ESI-MS: $[M+H]^+$ m/z calcd for $C_{40}H_{27}N_2O_2$: 567.20670, found: 567.20704; elemental analysis calcd (%) for $C_{40}H_{26}N_2O_2$: C 84.78, H 4.62, N 4.94; found: C 84.68, H 4.71, N 4.86.

Synthesis of 2-(4-bibenzothiophene-4-phenyl)-1-(4-methoxyphenyl)-1*H*-phenanthro[9,10-d]imidazole (PhImTD)

The procedure for **PhImTD** was similar as the preparation of **PhImFD** starting from **TD4B** (310.2 mg, 1 mmol) instead of **FD4B**. Yield: 79%. ^{1}H NMR (TMS, $CDCl_3$, 500 MHz): ppm δ = 3.96 (s, 3H), 7.14 (d, *J*=8.5 Hz, 2H), 7.28–7.43 (m, 4H), 7.46–7.54(m, 4H), 7.61(d, *J*=9.0 Hz, 2H), 7.66(t, *J*=7.5 Hz, 1H), 7.76 (t, *J*=7.0 Hz,1H), 7.81 (d, *J*=8.0 Hz,2H), 7.92 (dd, *J*=7.0 Hz, 3H), 7.98 (d, *J*=8.0 Hz, 1H), 8.71 (d, *J*=8.5 Hz, 1H), 8.78 (d, *J*=8.5 Hz, 1H), 8.93 (d, *J*=8.0 Hz, 1H); ^{13}C NMR (TMS, $CDCl_3$, 125 MHz): ppm δ = 160.50, 156.09, 153.45, 150.67, 136.55, 131.32, 130.18, 129.51, 129.31, 128.57, 128.50, 128.32, 127.30, 126.68, 126.32, 125.61, 124.88, 124.12, 123.23, 123.11, 122.85, 120.90, 120.69, 119.98, 115.38, 111.64, 55.70; HR-ESI-MS: $[M+H]^+$ m/z calcd for $C_{40}H_{27}N_2OS$: 583.18386, found: 583.18331; elemental analysis calcd (%) for $C_{40}H_{26}N_2OS$: C 82.45, H 4.50, N 4.81, S 5.50; found: C 82.33, H 4.47, N 4.75, S 5.62.

Conclusion

In conclusion, we have presented in this work the use of blue-fluorescent **PhImFD** and **PhImTD** containing the *n*-type imidazole moiety and *p*-type dibenzofuran or dibenzothiophene moiety for EL devices. Through DFT investigation, the bipolar units exist in the twisting D–A molecules connected by means of a freely *para*-linkage benzene ring. In addition, the unsymmetrical configuration adopts the

View Article Online
DOI: 10.1039/C5RA13814K

conjunction of dibenzofuran and dibenzothiophene units by C-4 positions could suppress strong π–π stacking and molecular interactions, which is attributed to the observed high quantum efficiency and thermal stability. With the similar optical properties and FMO locations, the effective utilization of **PhImTD** as the non-doped emitter, we demonstrate deep blue (CIE coordintaes: (0.15, 0.10)) electroluminescence device exhibits EQE of 1.63%, PE of 0.82 lm W^{-1} and CE of 1.34 cd m^{-1}. Appropriate bandgap endows blue devices with a low driving voltage of 3.6 V. Meanwhile, the WOLED devices using **PhImFD** and **PhImTD** as the host and yellow PO-01 as the dopant is realized with a maximum CE of 8.12 cd A^{-1} and CIE coordinates of (0.339, 0.330). This work indicated that compared to dibenzofuran as the electron-donating, the rational modulation by dibenzothiophene group is more strongly influence the energy level match for achieving materials with desired optoelectronic properties.

Acknowledgments

The authors greatly appreciate the financially supported by Chinese National Programs for Scientific Instruments Research and Development (No. 2012YQ03007502), National Science Foundation of China (No. 11090330) and China Postdoctoral Science Foundation (No. 2015T80018).

Notes and references

1. (a) M. C. Gather, A. Köhnen and K. Meerholz, *Adv. Mater.,* 2011**, 23**, 233; (b) S. Gong, C. Yang and J. Qin, *Chem. Soc. Rev.,* 2012**, 41**, 4797.
2. K. Udagawa, H. Sasabe, C. Cai and J. Kido, *Adv. Mater.,* 2014**, 26**, 5062.
3. (a) T. Keawin, C. Sooksai, N. Prachumrak, T. Kaewpuang, D. Muenmart, S. Namuangruk, S. Jungsuttiwong, T. Sudyoadsuk and V. Promarak, *RSC Adv.,* 2015, **5**, 16422; (b) Y. J. Kang, S. K. Jeon and J. Y. Lee, *Dyes Pigm.,* 2015, **114**, 278.
4. C. H. Chang, M. C. Kuo, W. C. Lin, Y. T. Chen, K. T. Wong, S. H. Chou, E. Mondal, R. C. Kwong, S. Xia, T. Nakagawa and C. Adachi, *J. Mater. Chem.,*

View Article Online
DOI: 10.1039/C5RA13814K

2012, **22**, 3832.

5. (a) J. H. Lee, S. H. Cheng, S. J. Yoo, H. Shin, J. H. Chang, C. I. Wu, K. T. Wong and J. J. Kim, *Adv. Funct. Mater.,* 2015, **25**, 361; (b) Q. Wang, I. W. H. Oswald, X. Yang, G. Zhou, H. Jia, Q. Qiao, Y. Chen, J. Hoshikawa-Halbert and B. E. Gnade, *Adv. Mater.,* 2014, **26**, 8107; (c) C. Tang, R. Bi, Y. Tao, F. Wang, X. Cao, S. Wang, T. Jiang, C. Zhong, H. Zhang and W. Huang, *Chem. Commun.,* 2015, **51**, 1650.
6. (a) Z. Jiang, Z. Zhong, S. Xue, Y. Zhou, Y. Meng, Z. Hu, N. Ai, J. Wang, L. Wang, J. Peng, Y. Ma, J. Pei, J. Wang and Y. Cao, *ACS Appl. Mater. Inter.,* 2014, **6**, 8345; (b) Y. L. Chang, Y. Song, Z. Wang, M. G. Helander, J. Qiu, L. Chai, Z. Liu, G. D. Scholes and Z. Lu, *Adv. Funct. Mater.,* 2013, **23**, 705; (c) T. Higuchi, H. Nakanotani and C. Adachi, *Adv. Mater.,* 2015, **27**, 2019.
7. G. Gu, Z. Sken, P. E. Burrows and S. R. Forrest, *Adv. Mater.*, 1997, **9**, 725.
8. (a) Y. Chi and P. T. Chou, *Chem. Soc. Rev.,* 2010, **39**, 638; (b) C. Ulbricht, B. Beyer, C. Friebe, A. Winter and U. S. Schubert, *Adv. Mater.,* 2009, **21**, 4418.
9. M. Zhu and C. Yang, *Chem. Soc. Rev.,* 2013, **42**, 4963.
10. (a) X. D. Yuan, J. Liang, Y. C. He, Q. Li, C. Zhong, Z. Q. Jiang and L. S. Liao, *J. Mater. Chem. C,* 2014, **2**, 6387; (b) S. Gong, Y. L. Chang, K. Wu, R. White, Z. H. Lu, D. Song and C. Yang, *Chem. Mater.,* 2014, **26**, 1463; (c) X. Wang, S. Wang, Z. Ma, J. Ding, L. Wang, X. Jing and F. Wang, *Adv. Func.Mater.,* 2014, **24**, 3413.
11. (a) C. J. Kuo, T. Y. Li, C. C. Lien, C. H. Liu, F. I. Wu and M. J. Huang, *J. Mater. Chem.,* 2009, **19**, 1865; (b) Z. M. Wang, X. H. Song, Z. Gao, D. W. Yu, X. J. Zhang, P. Lu, F. Z. Shen and Y. G. Ma, *RSC Adv.,* 2012, **2**, 9635; (c) S. Zhuang, R. Shangguan, J. Jin, G. Tu, L. Wang, J. Chen, D. Ma and X. Zhu, *Org. Electron.,* 2012, **13**, 3050; (d) Z. Gao, Y. Liu, Z. Wang , F. Shen, H. Liu, G. Sun, L. Yao, Y. Lv, P. Lu and Y. Ma, *Chem.–Eur. J.,* 2013, **19**, 2602; (e) D. Kumar, K. R. J. Thomas, C. C. Lin and J. H. Jou, *Chem.–Asian J.,* 2013, **8**, 2111.
12. (a) Y. Zhang, T. W. Ng, F. Lu, Q. X. Tong, S. L. Lai, M. Y. Chan, H. L. Kwong and C. S. Lee, *Dyes Pigm.,* 2013, **98**, 190; (b) W. C. Chen, Y. Yuan, G. F. Wu, H. X. Wei, L. Tang, Q. X. Tong, F. L. Wong and C. S. Lee, *Adv. Opt. Mater.,* 2014, **2**, 626; (c) J. Jayabharathi, R. Sathishkumar, V. Thanikachalam and K. Jayamoorthy,

View Article Online
DOI: 10.1039/C5RA13814K

J. Lumin., 2014, **153**, 343.

13. (a) S. Zhang, L. Yao, Q. Peng, W. Li, Y. Pan, R. Xiao, Y. Gao, C. Gu, Z. Wang, P. Lu, F. Li, S. Su, B. Yang and Y. Ma, *Adv. Funct. Mater.,* 2015, **25**, 1755; (b) L. Zheng and R. Hua, *J. Org. Chem.,* 2014, **79**, 3930.
14. (a) X. Yang, R. A. Jones, M. M. Oye, M. Wiester and R. J. Lai, *New J. Chem.,* 2011, **35**, 310; (b) S. Chen, R.-Q. Fan, X.-M. Wang and Y.-L. Yang, *CrystEngComm,* 2014, **16**, 6114.
15. C. Han, Z. Zhang, H. Xu, S. Yue, J. Li, P. Yan, Z. Deng, Y. Zhao, P. Yan and S. Liu, *J. Am. Chem. Soc.,* 2012, **134**, 19179.
16. Z. Wang, Y. Feng, H. Li, Z. Gao, X. Zhang, P. Lu, P. Chen, Y. Ma and S. Liu, *Phys. Chem. Chem. Phys.,* 2014, **16**, 10837.
17. (a) S. Anbu, S. Kamalraj, A. Paul, C. Jayabaskaran and A. J. L. Pombeiro, *Dalton Trans.,* 2015, **44** 3930; (b) W. C. Chen, G. F. Wu, Y. Yuan, H. X. Wei, F. L. Wong, Q. X. Tong and C. S. Lee, *RSC Adv.,* 2015, **5**, 18067; (c) M. Zhu, T. Ye, C. G. Li, X. Cao, C. Zhong, D. Ma, J. Qin, and C. Yang, *J. Phy. Chem. C,* 2011, **115**, 17965.
18. C. Liu, Q. Fu, Y. Zou, C. Yang, D. Ma and J. Qin, *Chem. Mater.,* 2014, **26**, 3074.
19. (a) D. Yu, F. Zhao, C. Han, H. Xu, J. Li, Z. Zhang, Z. Deng, D. Ma and P. Yan, *Adv. Mater.,* 2012, **24**, 509; (b) D. Yu, F. Zhao, Z. Zhang, C. Han, H. Xu, J. Li, D. Ma and P. Yan, *Chem. Commun.,* 2012, **48**, 6157.
20. Y. Yuan, J. X. Chen, W. C. Chen, S. F. Ni, H. X. Wei, J.Ye, F. L. Wong, Z. W. Zhou, Q. X. Tong and C. S. Lee, *Org. Electron.,* 2015, **18**, 61.
21. Y. Yuan, D. Li, X. Zhang, X. Zhao, Y. Liu, J. Zhang and Y. Wang, *New J. Chem.,* 2011, **35**, 1534.
22. W. Q. Zhou, H. P. Peng, J. K. Xu, H. Y. Xia and S. Z. Pu, *Polym. Int.*, 2008, **57**, 92.
23. C. Han, Z. Zhang, H. Xu, J. Li, G.Xie, R. Chen, Y. Zhao and W. Huang, *Angew. Chem., Int. Ed.,* 2012, **51**, 10104.
24. Z. Gao, Z. Wang, T. Shan, Y. Liu, F. Shen, Y. Pan, H. Zhang, X. He, P. Lu, B. Yang and Y. Ma, *Org. Electron.*, 2014, **15**, 2667.

View Article Online
DOI: 10.1039/C5RA13814K

25. H. H. Chou, Y. H. Chen, H. P. Hsu, W. H. Chang, Y. H. Chen and C. H. Cheng, *Adv. Mater.,* 2012, **24**, 5867.

26. Q. Zhang, J. Li, K. Shizu, S. Huang S. Hirata, H. Miyazaki and C. Adachi, *J. Am. Chem. Soc.,* 2012, **134**, 14706.

27. M. J. Frisch, G. W. Trucks, H. B. Schlegel, G. E. Scuseria, M. A. Robb, J. R. Cheeseman, G. Scalmani, V. Barone, B. Mennucci, G. A. Petersson, H. Nakatsuji, M. Caricato, X. Li, H. P. Hratchian, A. F. Izmaylov, J. Bloino, G. Zheng, J. L. Sonnenberg, M. Hada, M. Ehara, K. Toyota, R. Fukuda, J. Hasegawa, M. Ishida, T. Nakajima, Y. Honda, O. Kitao, H. Nakai, T. Vreven, J. A. Montgomery Jr, J. E. Peralta, F. Ogliaro, M. Bearpark, J. J. Heyd, E. Brothers, K. N. Kudin, V. N. Staroverov, R. Kobayashi, J. Normand, K. Raghavachari, A. Rendell, J. C. Burant, S. S. Iyengar, J. Tomasi, M. Cossi, N. Rega, J. M. Millam, M. Klene, J. E. Knox, J. B. Cross, V. Bakken, C. Adamo, J. Jaramillo, R. Gomperts, R. E. Stratmann, O. Yazyev, A. J. Austin, R. Cammi, C. Pomelli, J. W. Ochterski, R. L. Martin, K. Morokuma, V. G. Zakrzewski, G. A. Voth, P. Salvador, J. J. Dannenberg, S. Dapprich, A. D. Daniels, Ö. Farkas, J. B. Foresman, J. V. Ortiz, J. Cioslowski, and D. J. Fox, *Gaussian 09*, *Revision A.02*, Gaussian, Inc., Wallingford CT, 2009.

28. A. D. Becke, *J. Chem. Phys*., 1993, **98**, 5648.

29. C. Lee, W. Yang and R. G. Parr, *Phys. Rev. B*, 1988, **37**, 785.

View Article Online
DOI: 10.1039/C5RA13814K

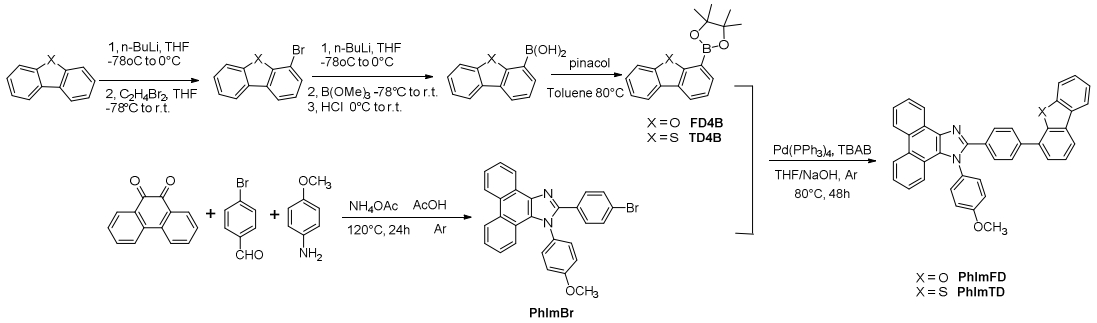

Scheme 1 Synthetic pathways toward bipolar molecules **PhImFD** and **PhImTD**.

View Article Online
DOI: 10.1039/C5RA13814K

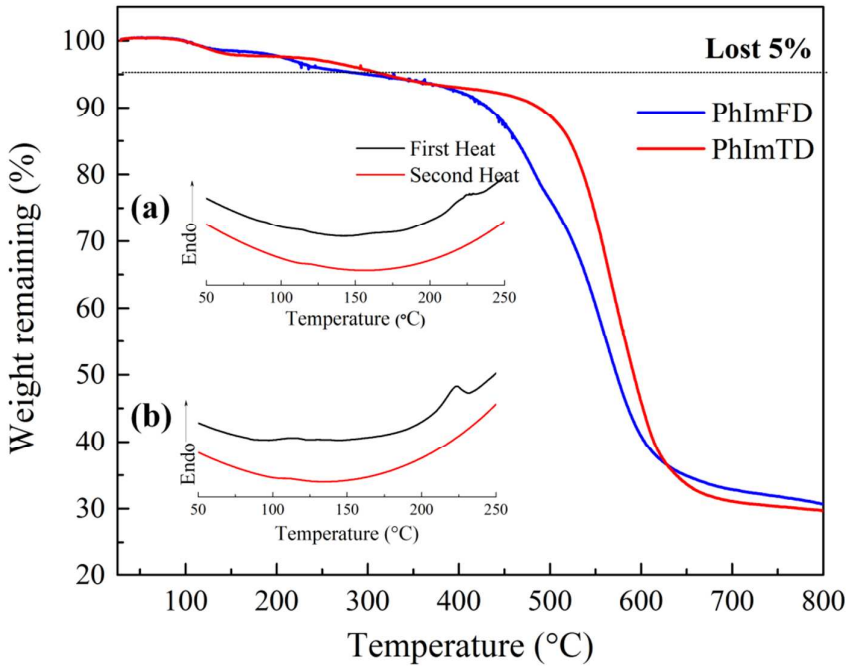

Fig. 1 TGA thermograms of **PhImFD** and **PhImTD**. Both at 10°C min^{-1} under notrogen flushing. Inset: DSC spectra of the first and second heating cyclings for **PhImFD** (a) and **PhImTD** (b) at a heating rate of 10 °C min^{-1} under notrogen flushing.

View Article Online
DOI: 10.1039/C5RA13814K

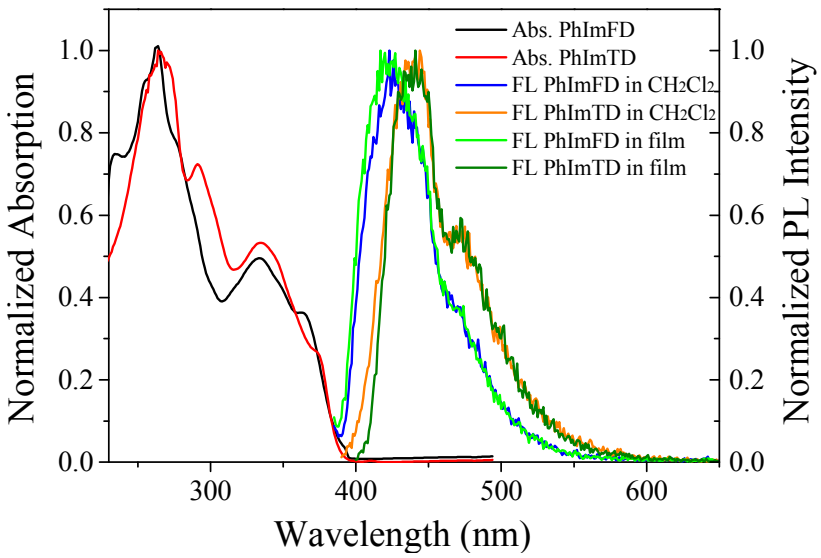

Fig. 2 Normalized UV-Vis absorption and fluorescence spectra of **PhImFD** and **PhImTD** in CH_2Cl_2 at 10^{-5} M and in spin-coating film at room temperature.

View Article Online
DOI: 10.1039/C5RA13814K

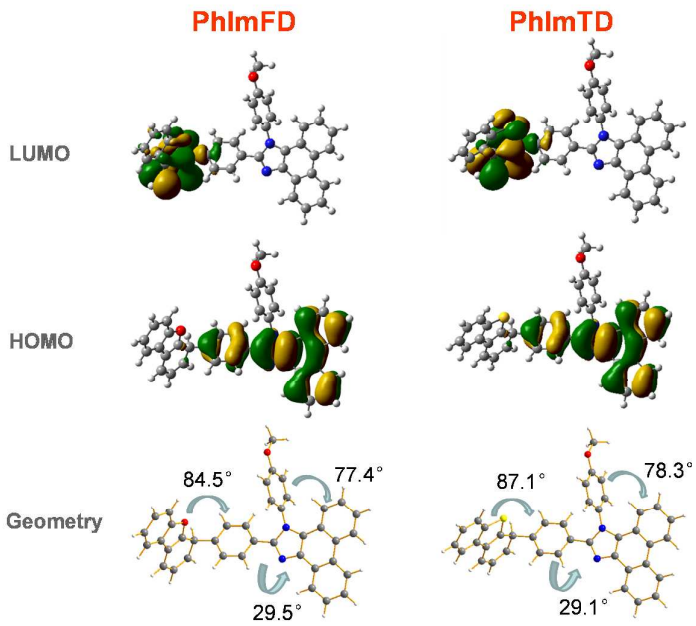

Fig. 3 FMOs (HOMO and LUMO) of **PhImFD** and **PhImTD** calculated with DFT on a B3LYP/6-31G(d) level.

View Article Online
DOI: 10.1039/C5RA13814K

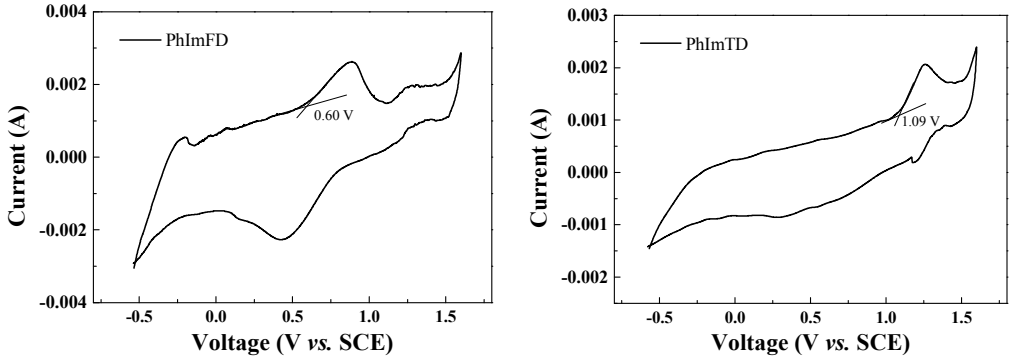

Fig. 4 Cyclic voltammogram of **PhImFD** and **PhImTD**. In each case, the anodic scan was performed in CH_2Cl_2 at a scan rate of 100 mV s^{-1}. The working electrode: platinum wire; the auxiliary electrode: platinum wire with a porous ceramic wick; the reference electrode: calomel electrode.

View Article Online
DOI: 10.1039/C5RA13814K

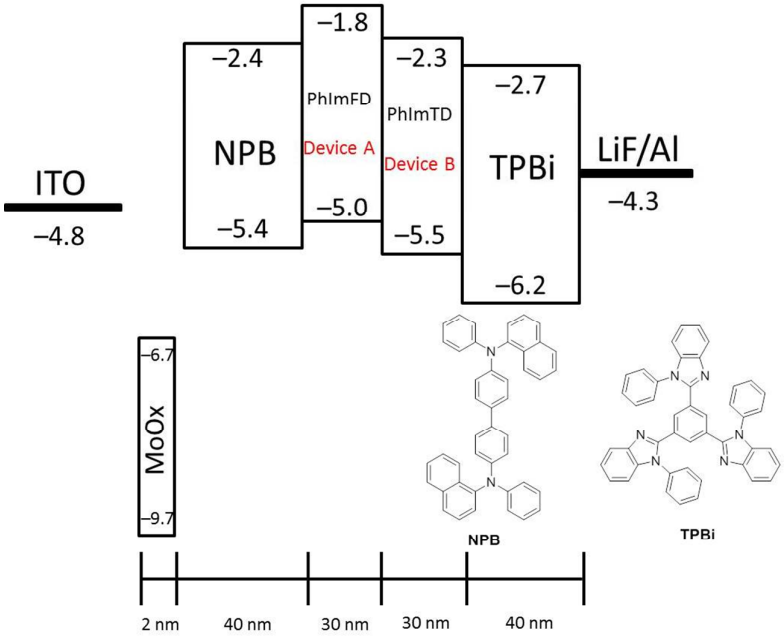

Fig. 5 Device structure and energy diagram of devices A and B.

View Article Online
DOI: 10.1039/C5RA13814K

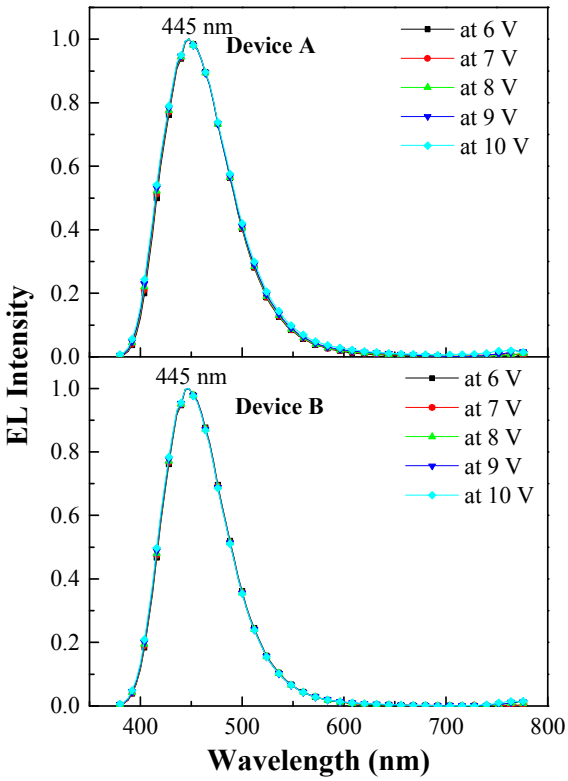

Fig. 6 Electroluminescence spectra for devices A and B at different voltages.

View Article Online
DOI: 10.1039/C5RA13814K

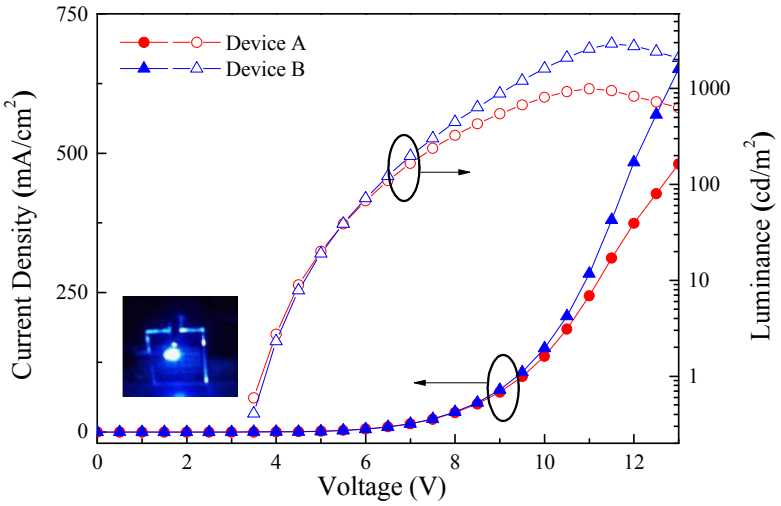

Fig. 7 Current density–voltage–luminance characteristics for devices A and B.

View Article Online
DOI: 10.1039/C5RA13814K

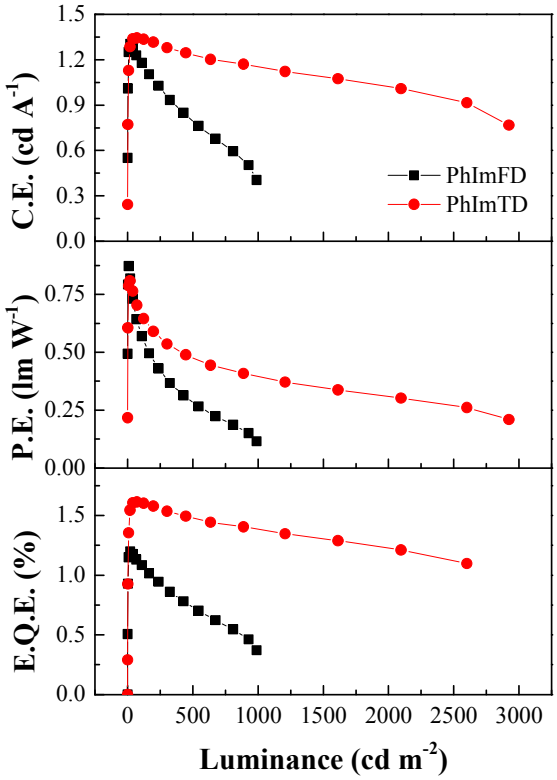

Fig. 8 Efficiency versus luminance curves of non-doped blue devices based on **PhImFD** and **PhImTD**.

View Article Online
DOI: 10.1039/C5RA13814K

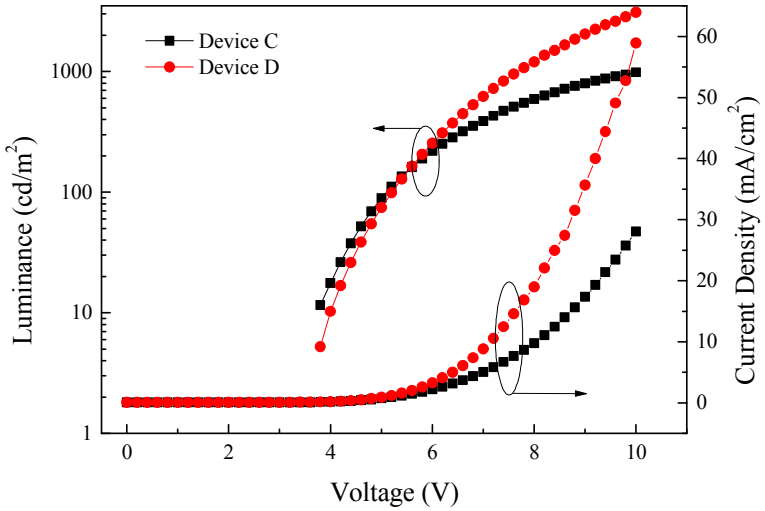

Fig. 9 Current density–voltage–luminance characteristics for devices C and D.

View Article Online
DOI: 10.1039/C5RA13814K

Table 1 The photophysical and thermal properties of **PhImFD** and **PhImTD**.

	$\lambda_{max,abs}$/nm [a]	$\lambda_{max,PL}$/nm [a]	$\lambda_{max,film}$/nm [b]	$\lambda_{max,\ ph}$/nm [c]	E_T/eV [d]	Tg/°C [e]	Td/°C [f]	HOMO/eV [g]	LUMO/eV [h]	Eg/eV [i]
PhImFD	263,280,333,364	421	440	476	2.68	110	300	5.00	1.81	3.19
PhImTD	265,292,334,374	423	440	477	2.70	115	318	5.49	2.32	3.17

[a] Measured in CH_2Cl_2 solution at room temperature;
[b] Measured in spin-coating film at room temperature;
[c] Measured in 2-methyl-THF glass matrix at 77 K;
[d] Estimated according to 0-0 transitions of time-resolved phosphorescent spectra;
[e] Tg: glass transition temperature, obtained from DSC measurements;
[f] Td: decomposition temperature at weight loss of 5%, obtained from TGA measurements;
[g] HOMO was calculated from the onset value of the oxidation potential;
[h] LUMO was calculated from the HOMO and the optical band gap Eg;
[i] Eg: the optical band gap was calculated from the absorption spectra.

View Article Online
DOI: 10.1039/C5RA13814K

Table 2 Key performance parameters of non-doped deep blue devices.

Material	Device	V_{on} (V)[a]	λ_{max} (nm)	FWHM (nm)	CE_{max}[b] (cd A^{-1})	PE_{max}[b] (lm W^{-1})	EQE_{max}[b] (%)	CIE (x, y)[c]
PhImFD	A	3.6	445	73	1.31	0.88	1.21	(0.151, 0.115)
PhImTD	B	3.6	445	69	1.34	0.82	1.63	(0.151, 0.098)

[a] Voltage required for 1 cd m^{-2};

[b] current efficiency (CE_{max}), power efficiency (PE_{max}), external quantum yield (EQE_{max});

[c] The CIE are measured at 1000 cd m^{-2}.